



Lengthwise Fracture Analysis of Inhomogeneous Viscoelastic Cantilever Beam Subjected to Sinusoidal Strains

Victor RIZOV *University of Architecture, Civil Engineering and Geodesy, 1046 Sofia, Bulgaria*

Highlights

- This paper is focused on viscoelastic beam with a lengthwise crack under sinusoidal strains.
- A viscoelastic model for describing the behavior of the beam is presented.
- A parametric analysis of the influence of various factors on the lengthwise fracture is performed.

Article Info

Received: 25 Jan 2022
Accepted: 25 Apr 2023

Keywords

*Inhomogeneous beam
Lengthwise crack
Sinusoidal strain
Analytical approach
Viscoelastic behavior*

Abstract

This paper describes a research of lengthwise fracture in a viscoelastic inhomogeneous cantilever beam under strain that is a sinusoidal function of time. The beam mechanical behavior is investigated by a model having two linear springs and a linear dashpot. The beam material is continuously inhomogeneous along thickness. Therefore, the modules of elasticity of the springs and the coefficient of viscosity of the dashpot vary smoothly in the thickness direction. The compliance method is applied to derive the strain energy release rate (SERR) for the lengthwise crack in the beam structure. The integral J is applied for verification. The stress-strain-time dependence of the viscoelastic model is used for describing the behavior of the beam when obtaining solutions of the SERR and the J -integral. Solutions are derived for both positive and negative rotation angle of the lower crack arm end (when the angle is positive, the upper crack arm is load free, while at negative angle both crack arms are loaded). The effects of various factors including the sign of the angle of rotation on the SERR are analyzed.

1. INTRODUCTION

The technical progress is inextricably bound up with utilization of various types of inhomogeneous structural materials in the recent years [1, 2]. Among them, the materials with continuous inhomogeneity are very attractive for both scientists and practicing engineers. Their properties are smooth functions of one or more coordinates. One of the most efficient materials of this type is the functionally graded material (FGM) [3-7]. The concept of FGM is developed originally in Japan in year 1984. The FGM represents a continuous mix of several materials. The composition of FGM changes smoothly within the structural member [8-15]. The basic idea is by varying continuously the microstructure of the material with a definite gradient along one or more spatial coordinates to manufacture a composite material with smoothly changing properties. The concept of FGM is very suitable for designing of materials aimed for use in specific structural applications [16-20]. Due to their superior properties, the FGM applied in aerospace industry, nuclear fusion reactors, biomedicine, automotive industry, etc. are an important factor for enhancing the operational reliability of facilities in these areas.

Studying fracture plays an essential role in design of engineering constructions made of continuously inhomogeneous (functionally graded) materials [21-24]. Failure of various load-bearing structures very often is due to appearance of cracks. Therefore, ensuring of durability and operational reliability of continuously inhomogeneous engineering constructions and facilities requires development and application of different fracture analyses in the process of structural design.

In their life-time, continuously inhomogeneous load-bearing structures often are under external loadings and influences which change according to a sinusoidal law. Also, these structures exhibit viscoelastic mechanical behaviour in their life-time that should be considered when analyzing fracture. In view of this, the current paper studies lengthwise fracture of a continuously inhomogeneous cantilever under sinusoidal strains. Viscoelastic behaviour is analyzed by a linear model. The stress-strain-time dependence under sinusoidal strains is derived. This dependence is used when obtaining solution of the SERR for the lengthwise crack. It should be mentioned that earlier lengthwise fracture studies deal with constant loading or loading that changes linearly with time [25, 26]. Hence, the novelty here is the consideration of the sinusoidal strains and their effects on the lengthwise crack.

2.VISCOELASTIC BEAM WITH LENGTHWISE CRACK SUBJECTED TO SINUSOIDAL STRAINS

The linear viscoelastic model under consideration is with two linear springs, E_D and E_H , and a linear dashpot, η , assembled as displayed in Figure 1.

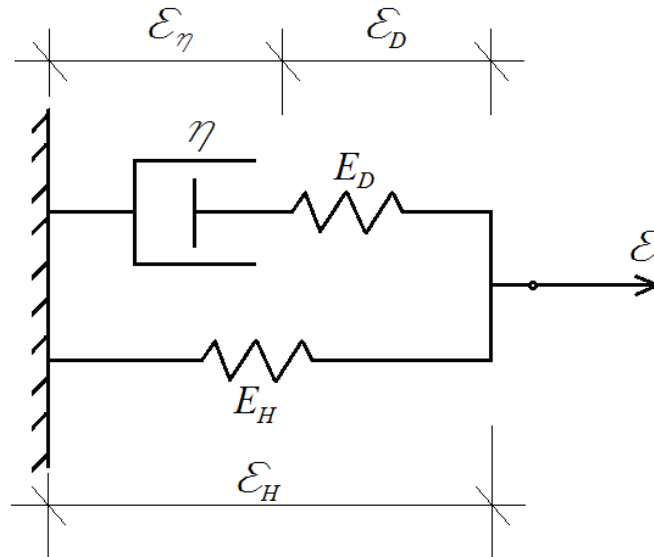


Figure 1. Viscoelastic model

The model strain is ε . The variation of strain with time, t , follows sinusoidal law

$$\varepsilon = \varepsilon_0 \sin(\omega t) \quad (1)$$

where ε_0 and ω are the amplitude and the angular frequency.

The relation between stress, strain and time for the viscoelastic model is derived by applying the following approach. First, relations between strains are written as

$$\varepsilon_\eta + \varepsilon_D = \varepsilon_H, \quad (2)$$

$$\varepsilon_H = \varepsilon \quad (3)$$

where ε_η , ε_D and ε_H are strains in the dashpot and in the springs, respectively (Figure 1).

The equations of equilibrium of the components of the model are obtained as

$$\sigma_{\eta} + \sigma_H = \sigma, \quad (4)$$

$$\sigma_{\eta} = \sigma_D \quad (5)$$

where σ_{η} , σ_D and σ_H are the stresses.

They are expressed as

$$\sigma_{\eta} = \eta \dot{\varepsilon}_{\eta}, \quad (6)$$

$$\sigma_D = E_D \varepsilon_D, \quad (7)$$

$$\sigma_H = E_H \varepsilon_H. \quad (8)$$

In formula (6), $\dot{\varepsilon}_{\eta}$ is the first derivative of ε_{η} .

By combining of (1) – (8) and performing some mathematical transformations, one obtains the following first-order linear inhomogeneous ordinary differential equation:

$$\dot{\varepsilon}_{\eta} + \beta \varepsilon_{\eta} = \delta \sin(\omega t) \quad (9)$$

where

$$\beta = \frac{E_D}{\eta}, \quad (10)$$

$$\delta = \beta \varepsilon_0. \quad (11)$$

Equation (9) is used to determine ε_{η} . In result, we have

$$\varepsilon_{\eta}(t) = C e^{-\beta t} + \bar{\varepsilon}_{\eta}. \quad (12)$$

Here C is an integration constant. $\bar{\varepsilon}_{\eta}$ is

$$\bar{\varepsilon}_{\eta} = \lambda \sin(\omega t) + \theta \cos(\omega t) \quad (13)$$

where λ and θ are constants. First, $\bar{\varepsilon}_{\eta}$ and its derivative are substituted in (9). Then, by some mathematical manipulations, one derives

$$(-\theta \omega + \beta \lambda - \delta) \sin(\omega t) + (\lambda \omega + \beta \theta) \cos(\omega t) = 0. \quad (14)$$

Equation (14) is satisfied when the expressions in brackets before $\sin(\omega t)$ and $\cos(\omega t)$ are equal to zero

$$-\theta\omega + \beta\lambda - \delta = 0, \quad (15)$$

$$\lambda\omega + \beta\theta = 0. \quad (16)$$

Equations (15) and (16) are solved with respect to λ and θ . The result is

$$\lambda = \frac{\delta\beta}{\omega^2 + \beta^2}, \quad \theta = -\frac{\delta\omega}{\omega^2 + \beta^2}. \quad (17)$$

The initial condition used to determine the integration constant, C , is written as

$$\varepsilon_\eta(0) = 0. \quad (18)$$

Thus, C is found as

$$C = -\theta. \quad (19)$$

In this way, the solution of (9) takes the form

$$\varepsilon_\eta(t) = -\theta e^{-\beta t} + \lambda \sin(\omega t) + \theta \cos(\omega t). \quad (20)$$

By combining of (6) and (20), one derives

$$\sigma_\eta(t) = \eta [\theta\beta e^{-\beta t} + \lambda\omega \cos(\omega t) - \theta\omega \sin(\omega t)]. \quad (21)$$

By using (1), (3) and (8), one obtains

$$\sigma_H(t) = E_H \varepsilon_0 \sin(\omega t). \quad (22)$$

Combination of (21), (22) and (4) yields the following dependence for the linear viscoelastic model under consideration (Figure 1):

$$\begin{aligned} \sigma(t) = & \eta [\theta\beta e^{-\beta t} + \lambda\omega \cos(\omega t) - \theta\omega \sin(\omega t)] \\ & + E_H \varepsilon_0 \sin(\omega t). \end{aligned} \quad (23)$$

Dependence (23) is used for describing the behaviour of the beam structure displayed in Figure 2. The structure under consideration is clamped. The sizes of the structure are b , h and l . There is a lengthwise crack in the structure. The crack length is a . The crack arms thicknesses are h_1 and h_2 .

The lower arm of the crack is subjected to bending. The angle of rotation, φ , is sinusoidal function of time

$$\varphi = \varphi_0 \sin(\omega t) \quad (24)$$

where φ_0 is the amplitude. The positive direction of φ is displayed in Figure 2.

The properties of the material change along the beam thickness.

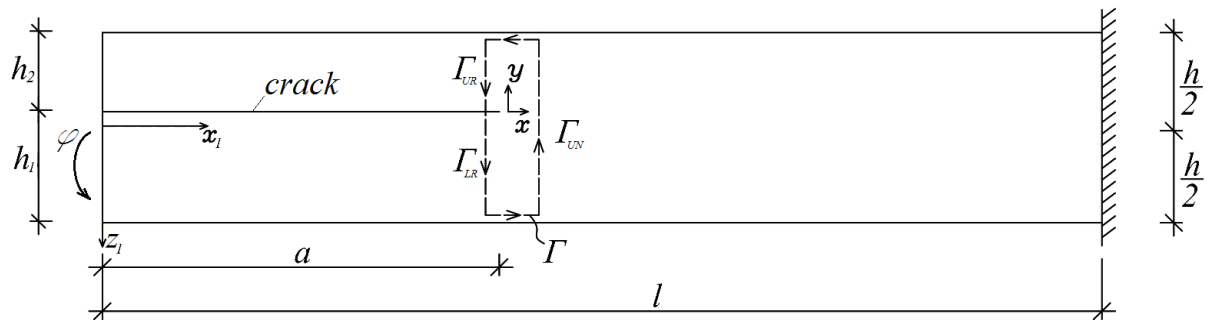


Figure 2. Inhomogeneous beam with lengthwise crack

Change of η , E_D and E_H along the thickness of the beam is

$$\eta = \eta_R + \frac{\eta_S - \eta_R}{h^{f_\eta}} \left(\frac{h}{2} + z_1 \right)^{f_\eta}, \quad (25)$$

$$E_D = E_{DR} + \frac{E_{DS} - E_{DR}}{h^{f_D}} \left(\frac{h}{2} + z_1 \right)^{f_D}, \quad (26)$$

$$E_H = E_{HR} + \frac{E_{HS} - E_{HR}}{h^{f_H}} \left(\frac{h}{2} + z_1 \right)^{f_H} \quad (27)$$

where

$$-\frac{h}{2} \leq z_1 \leq \frac{h}{2}. \quad (28)$$

In formulae (25) – (28), z_1 is the beam vertical centric axis. Formulae (25) – (28) indicate that values of η , E_D and E_H change from η_R , E_{DR} and E_{HR} to η_S , E_{DS} and E_{HS} . The quantities, f_η , f_D and f_H , in (25) – (28) control the distribution of η , E_D and E_H , respectively.

As already mentioned, this paper aims to derive a solution of SERR for beam in Figure 2. The compliance method is applied. Therefore, the SERR, G , is written as

$$G = \frac{M^2}{2b} \frac{dC}{da} \quad (29)$$

where C and M are the beam compliance and the moment at the free end. The compliance is

$$C = \frac{\varphi}{M}. \quad (30)$$

The moments is

$$M = b \int_{-\frac{h_1}{2}}^{\frac{h_1}{2}} \sigma_{z_2} dz_2 \quad (31)$$

where z_2 is the lower crack arm centric axis.

In order to proceed further, stress, σ , is presented as a function of z_2 . First, the variation of strains is studied. Application of Bernoulli's hypothesis yields

$$\varepsilon = \kappa_{LR}(z_2 - z_{2n}) \quad (32)$$

where

$$-\frac{h_1}{2} \leq z_2 \leq \frac{h_1}{2}. \quad (33)$$

In formulae (32) and (33), κ_{LR} is the curvature, z_{2n} is the neutral axis coordinate. The hypothesis of Bernoulli is applicable because beam length to thickness ratio is high.

By combining of (11), (16), (17), (23), (24) and (32), one drives the following expression for the stress:

$$\sigma(t) = \frac{\kappa_{LR}(z_2 - z_{2n})}{\sin(\omega t)} \left\{ \eta \left[\theta_\rho \beta e^{-\beta t} + \lambda_\rho \omega \cos(\omega t) - \theta_\rho \omega \sin(\omega t) \right] + E_H \sin(\omega t) \right\} \quad (34)$$

where

$$\theta_\rho = -\frac{\beta \omega}{\omega^2 + \beta^2}, \quad (35)$$

$$\lambda_\rho = \frac{\beta^2}{\omega^2 + \beta^2}. \quad (36)$$

Determination of κ_{LR} and z_{2n} is the next step. One of the important peculiarities of the current analysis is that φ changes periodically its sign (this follows from formula (24)). According to (24), at

$$(m-1)\pi \leq \omega t \leq m\pi, \quad m = 1, 3, 5, 7, \dots \quad (37)$$

the sign of φ is positive. At

$$m\pi \leq \omega t \leq (m+1)\pi, \quad m = 1, 3, 5, 7, \dots \quad (38)$$

the angle φ has a negative sign.

When the sign of φ is positive, the upper crack arm is not loaded since the lower crack arm is rotated anticlockwise and bending moment can not be transmitted to the upper crack arm. However, when the sign of φ is negative, two crack arms are in contact. Therefore, both crack arms are loaded (their curvature is the same).

First, the curvature and the neutral axis coordinate are found for case when φ is positive. For this purpose, fact that the axial forces are zero is used to write two equations

$$b \int_{-\frac{h_1}{2}}^{\frac{h_1}{2}} \sigma dz_2 = 0, \quad (39)$$

$$b \int_{-\frac{h}{2}}^{\frac{h}{2}} \sigma_{UN} dz_3 = 0 \quad (40)$$

where σ_{UN} is the stress in portion, $a \leq 0 \leq l$. The quantities, κ_{LR} , z_2 and z_{2n} , are replaced with κ_{UN} , z_3 and z_{3n} in (34) to obtain σ_{UN} . Here, κ_{UN} , z_3 and z_{3n} are the curvature, centric axis and the coordinate of the neutral axis.

The equilibrium of moments is expressed as

$$b \int_{-\frac{h_1}{2}}^{\frac{h_1}{2}} \sigma \left(\frac{h}{2} - \frac{h_1}{2} + z_2 \right) dz_2 = b \int_{-\frac{h}{2}}^{\frac{h}{2}} \sigma_{UN} z_3 dz_3. \quad (41)$$

φ is found by the integrals of Maxwell-Mohr

$$\varphi = \kappa_{LR} a + \kappa_{UN} (l - a). \quad (42)$$

Equations (39) – (42) are solved for κ_{LR} , z_{2n} , κ_{UN} and z_{3n} by the MatLab.

For case of negative angle, φ , the following six equations are compiled:

$$b \int_{-\frac{h_1}{2}}^{\frac{h_1}{2}} \sigma dz_2 = 0, \quad (43)$$

$$b \int_{-\frac{h}{2}}^{\frac{h}{2}} \sigma_{UN} dz_3 = 0, \quad (44)$$

$$b \int_{-\frac{h_2}{2}}^{\frac{h_2}{2}} \sigma_{UR} dz_4 = 0 \quad (45)$$

where σ_{UR} is the stress. The quantities, κ_{LR} , z_2 and z_{2n} , are replaced with κ_{UR} , z_4 and z_{4n} in (34) to obtain σ_{UR} (κ_{UR} , z_4 and z_{4n} are the curvature, centric axis and the coordinate of the neutral axis, respectively).

The bending moments are in equilibrium

$$b \int_{-\frac{h_1}{2}}^{\frac{h_1}{2}} \sigma \left(\frac{h}{2} - \frac{h_1}{2} + z_2 \right) dz_2 + \quad (46)$$

$$b \int_{-\frac{h_2}{2}}^{\frac{h_2}{2}} \sigma_{UR} \left(-\frac{h}{2} + \frac{h_1}{2} + z_4 \right) dz_4 = b \int_{-\frac{h}{2}}^{\frac{h}{2}} \sigma_{UN} z_3 dz_3.$$

The two crack arms have the same curvature

$$\kappa_{LR} = \kappa_{UR}. \quad (47)$$

After substituting of stresses in (43) – (46), these equations are solved with (42) and (46) for κ_{LR} , z_{2n} , κ_{UN} , z_{3n} , κ_{UR} and z_{4n} .

By substituting of (30), (31) and (42) in (29), the SERR is found as

$$G = \frac{\kappa_{LR} - \kappa_{UN}}{2} \int_{-\frac{h_1}{2}}^{\frac{h_1}{2}} \sigma z_2 dz_2. \quad (48)$$

The lengthwise crack problem displayed in Figure 2 is treated also by the J -integral [27] for check-up of (48). Contour, Γ , is used for integration (Figure 2). It is found that

$$J = J_{\Gamma_{LR}} + J_{\Gamma_{UN}} + J_{\Gamma_{UR}} \quad (49)$$

where $J_{\Gamma_{LR}}$, $J_{\Gamma_{UN}}$ and $J_{\Gamma_{UR}}$ are the values in parts, Γ_{LR} , Γ_{UN} and Γ_{UR} , of the integration contour, respectively (Figure 2).

Expression for $J_{\Gamma_{LR}}$ is written as

$$J_{\Gamma_{LR}} = \int_{\Gamma_{LR}} \left[u_{0LR} \cos \alpha_{\Gamma_{LR}} - \left(p_{x_{\Gamma_{LR}}} \frac{\partial u}{\partial x} + p_{y_{\Gamma_{LR}}} \frac{\partial v}{\partial x} \right) \right] ds_{\Gamma_{LR}} \quad (50)$$

where u_{0LR} is

$$u_{0LR} = \frac{1}{2} \sigma \varepsilon. \quad (51)$$

Substitution of (32) and (34) in (51) yields

$$u_{0LR} = \frac{[\kappa_{LR}(z_2 - z_{2n})]^2}{2 \sin(\omega t)} \left\{ \eta \left[\theta_\rho \beta e^{-\beta t} + \lambda_\rho \omega \cos(\omega t) - \theta_\rho \omega \sin(\omega t) E \right] + E_H \sin(\omega t) \right\} \quad (52)$$

Other components of (50) are found as

$$\cos \alpha_{\Gamma_{LR}} = -1, \quad (53)$$

$$p_{x_{\Gamma_{LR}}} = -\sigma, \quad (54)$$

$$p_{y_{\Gamma_{LR}}} = 0, \quad (55)$$

$$ds_{\Gamma_{LR}} = dz_2, \quad (56)$$

$$\frac{\partial u}{\partial x} = \varepsilon. \quad (57)$$

It should be noted that $z_2 \in [-h_1/2; h_1/2]$.

In part, Γ_{UN} , of the contour it is found that

$$J_{\Gamma_{UN}} = \int_{\Gamma_{UN}} \left[u_{0UN} \cos \alpha_{\Gamma_{UN}} - \left(p_{x_{\Gamma_{UN}}} \frac{\partial u}{\partial x} + p_{y_{\Gamma_{UN}}} \frac{\partial v}{\partial x} \right) \right] ds_{\Gamma_{UN}} \quad (58)$$

where u_{0UN} is found by (52) (formula (52) is modified by replacing of κ_{LR} , z_2 and z_{2n} with κ_{UN} , z_3 and z_{3n}). The rest of the components of (58) are written as

$$\cos \alpha_{\Gamma_{UN}} = 1, \quad (59)$$

$$p_{x_{\Gamma_{UN}}} = \sigma_{UN}, \quad (60)$$

$$p_{y_{\Gamma_{UN}}} = 0, \quad (61)$$

$$ds_{\Gamma_{UN}} = dz_3, \quad (62)$$

$$\frac{\partial u}{\partial x} = \varepsilon_{UN} \quad (63)$$

where the strain, ε_{UN} , is found by replacing of κ_{LR} , z_2 and z_{2n} with κ_{UN} , z_3 and z_{3n} in formula (32). Besides, here z_3 changes in the interval $[h/2; -h/2]$.

In part, Γ_{UR} , we have

$$J_{\Gamma_{UR}} = \int_{\Gamma_{UR}} \left[u_{0UR} \cos \alpha_{\Gamma_{UR}} - \left(p_{x_{\Gamma_{UR}}} \frac{\partial u}{\partial x} + p_{y_{\Gamma_{UR}}} \frac{\partial v}{\partial x} \right) \right] ds_{\Gamma_{UR}} \quad (64)$$

where

$$\cos \alpha_{\Gamma_{UR}} = -1, \quad (65)$$

$$p_{x_{\Gamma_{UR}}} = -\sigma_{UR}, \quad (66)$$

$$p_{y_{\Gamma_{UR}}} = 0, \quad (67)$$

$$ds_{\Gamma_{UR}} = dz_4, \quad (68)$$

$$\frac{\partial u}{\partial x} = \varepsilon_{UR}. \quad (69)$$

Here, κ_{LR} , z_2 and z_{2n} are replaced with κ_{UR} , z_4 and z_{4n} in formula (32) to determine the strain, ε_{UR} . The coordinate, z_4 , changes in the interval $[-h_2/2; h_2/2]$.

The integrals (50), (58) and (64) are solved by MatLab. The J -integral yielded by (49) are matches of SERR found by (48) which is verification of (48).

3. PARAMETRIC ANALYSIS

Parametric analysis is developed here by calculating of the SERR with help of (48).

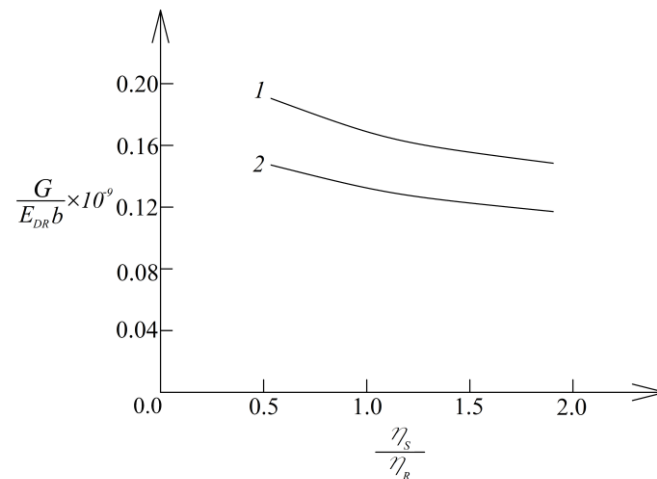


Figure 3. Dependence of the SERR on η_s / η_r ratio (curve 1 – at $\varphi = \varphi_0$, curve 2 – at $\varphi = -\varphi_0$)

The findings of the parametric analysis throw light upon the influence of various factors on the SERR for the lengthwise crack in the viscoelastic structure under sinusoidal strains for $b = 0.015$ m, $h = 0.010$ m, $l = 0.350$ m, $\omega = 0.05$ s⁻¹, $\varphi_0 = 0.03$ rad and $f_D = f_H = f_\eta = 0.8$.

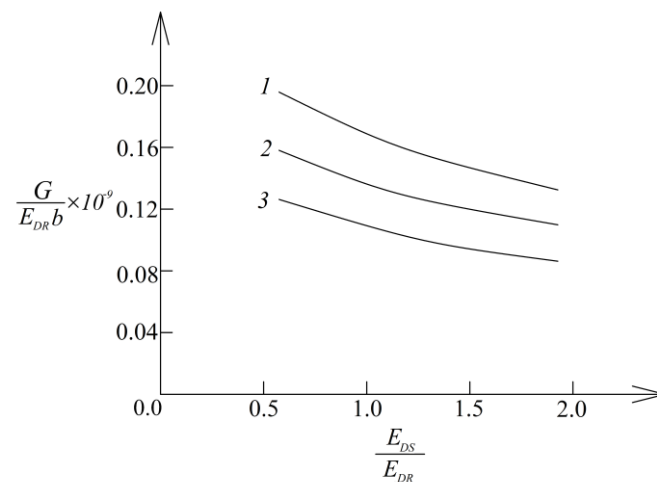


Figure 4. Dependence of the SERR on E_{DS} / E_{DR} ratio (curve 1 – at $h_1 / h = 0.2$, curve 2 – at $h_1 / h = 0.5$, curve 3 – at $h_1 / h = 0.7$)

First, influence of sign of angle of rotation, φ , on the SERR is studied. For this purpose, the SERR is obtained at $\varphi = \varphi_0$ and at $\varphi = -\varphi_0$.

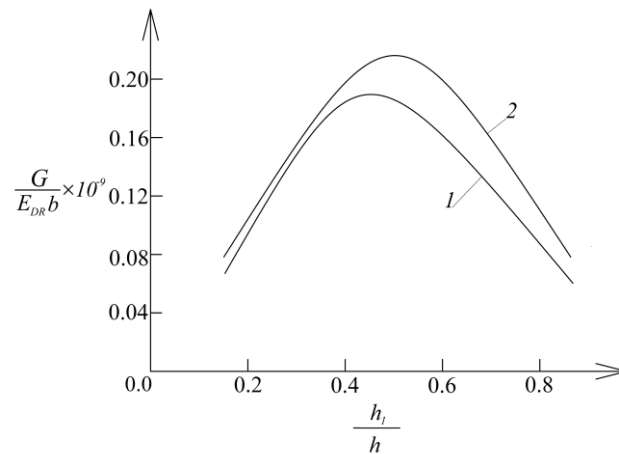


Figure 5. Dependence of the SERR on h_1/h ratio at $\varphi < 0$ (curve 1 – for inhomogeneous beam, curve 2 – for homogeneous beam)

The influence of the gradual change of η along the thickness is studied too. The results obtained are displayed in Figure 3 (the SERR is expressed as $G_N = G/(E_{DR}b)$). SERR at $\varphi = \varphi_0$ is higher than that at $\varphi = -\varphi_0$ (Figure 3). This is due to the fact that at $\varphi > 0$ the moment loads only lower crack arm, while at $\varphi < 0$ bending moment works on both crack arms. Increase of η_S/η_R ratio generates decrease of SERR (Figure 3).

The variation of the SERR with E_{DS}/E_{DR} and h_1/h ratios is also investigated (the first ratio characterizes the change of E_D). Dependence between the SERR and E_{DS}/E_{DR} ratio is displayed in Figure 4 for three h_1/h ratios.

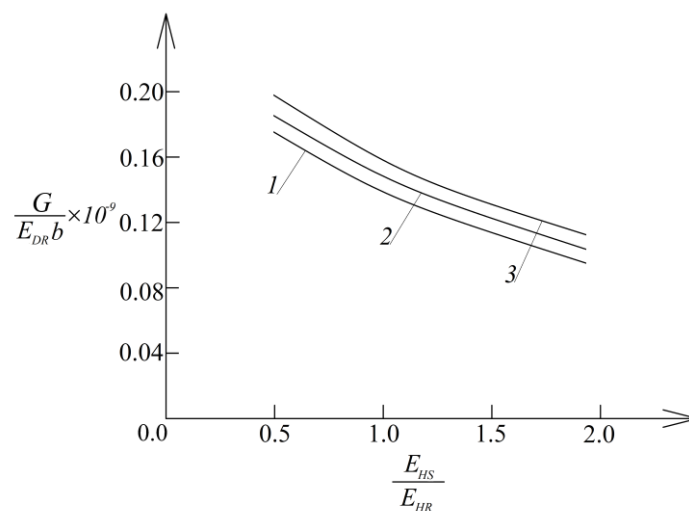


Figure 6. Dependence of the SERR on E_{HS}/E_{HR} ratio (curve 1 – at $f_H = 0.5$, curve 2 – at $f_H = 0.7$, curve 3 – at $f_H = 0.9$)

From Figure 4, it can be found that growth of E_{DS}/E_{DR} ratio generates decrease of the SERR. The SERR decreases when h_1/h ratio increases.

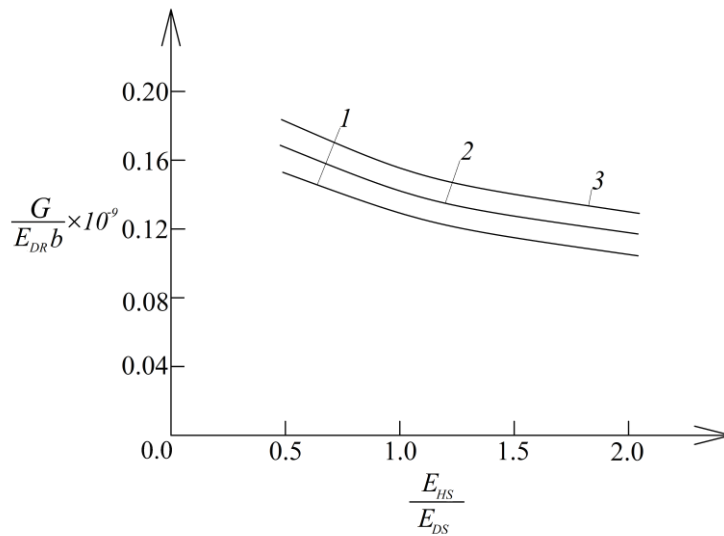


Figure 7. Dependence of the SERR on E_{HS} / E_{DS} ratio (curve 1 – at $f_D = 0.6$, curve 2 – at $f_D = 0.8$, curve 3 – at $f_D = 1.0$)

This finding is reasonable since the results displayed in Figure 4 are obtained at $\varphi > 0$. Growth of h_1 / h ratio induces augmentation of the stiffness which is reason for decrease of the SERR.

SERR is evaluated also at $\varphi < 0$. The dependence of the SERR on h_1 / h ratio in this case is displayed in Figure 5. It can be found from Figure 5 that the SERR has maximum when h_1 / h is near 0.5. Variation of SERR with h_1 / h ratio is evaluated also assuming that the beam under consideration is homogeneous. The dependence of the SERR on h_1 / h ratio for homogeneous beam is shown also in Figure 5. In homogeneous beam, the SERR has maximum at $h_1 / h = 0.5$ (Figure 5).

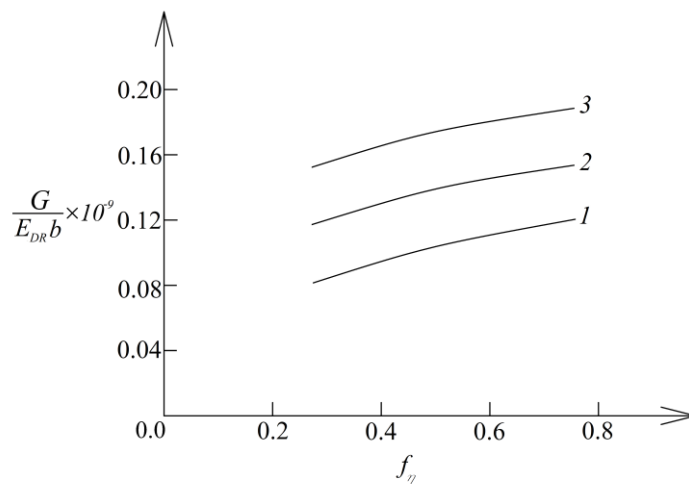


Figure 8. Dependence of the SERR on parameter f_n (curve 1 – at $\varphi_0 = 0.01$ rad, curve 2 – at $\varphi_0 = 0.02$ rad, curve 3 – at $\varphi_0 = 0.03$ rad)

Influence of change of E_H is analyzed. For this purpose, SERR is found at various E_{HS} / E_{HR} ratios. Figure 6 depicts the variation of the SERR with E_{HS} / E_{HR} ratio at three values of f_H . From Figure 6, one learns

that the SERR reduces with the increase of E_{HS} / E_{HR} ratio. It can be seen also that SERR grows with rise of the parameter f_H (Figure 6).

Figure 7 illustrates the change of SERR with rise of E_{HS} / E_{DS} ratio at three values of the parameter, f_D . It can be noticed that SERR decreases with rise of E_{HS} / E_{DS} . Rise of parameter, f_D , induces increase of SERR (Figure 7).

Variation of SERR with growth of f_η is depicted in Figure 8 for three amplitudes, φ_0 , of the angle of rotation. Growth of f_η induces rise of SERR (Figure 8). Curves in Figure 8 show that SERR increases with growth of φ_0 .

4. RESULTS

Lengthwise fracture of a linear viscoelastic inhomogeneous beam structure subjected to strain varying with time according to sinusoidal law is analyzed. A viscoelastic model with a dashpot and two springs is adopted for treating time-dependent behaviour of the structure. The connection between stress, strain and time of the model is derived and applied when analyzing SERR for the lengthwise crack. The lower crack arm is under bending so that its free end rotates according to sinusoidal law. One important peculiarity of the present crack problem is the fact that at positive angle of rotation the upper crack arm is stress free. At negative angle of rotation, however, both crack arms are loaded since the moment acts upon both crack arms. The compliance method is exercised to solve SERR problem for positive and negative angle of rotation. The integral J is applied for verification of SERR. A parametric analysis of SERR is carried-out. It is found that at negative angle of rotation SERR is lower than that at positive angle (this can be explained with the fact that at negative angle of rotation, the bending moment loads both crack arms). The influence of the continuous change of modules of elasticity and the coefficient of viscosity is explored. SERR diminishes with rising of η_S / η_R , E_{DS} / E_{DR} , E_{HS} / E_{HR} and E_{HS} / E_{DS} ratios. The growth of parameters, f_H , f_D and f_η , induces rise of SERR. Analysis reveals that at $\varphi > 0$ SERR diminishes with growth of h_1 / h ratio. However, at $\varphi < 0$ SERR has maximum when h_1 / h is near 0.5. SERR grows with rising of the amplitude of the angle of rotation.

CONFLICTS OF INTEREST

No conflict of interest was declared by the author.

REFERENCES

- [1] Karacor, B., Özcanlı, M., "Examination of Fiber Reinforced Composite Materials", Gazi University Journal of Science, 36(1): 301-320, (2023).
- [2] Özdemir, A.O., Subaşı, M., Karataş, Ç., "Investigating the Effects of Forming Parameters on Molding Force and Springback in Deep Drawing Process of Thermoplastic Composite Laminates", Gazi University Journal of Science, 34(2): 506-515, (2021).
- [3] Hirai, T., Chen, L., "Recent and prospective development of functionally graded materials in Japan", Mater Science Forum, 308-311(4): 509-514, (1999).
- [4] Butcher, R.J., Rousseau, C.E., Tippur, H.V., "A functionally graded particulate composite: Measurements and Failure Analysis", Acta Materialia, 47(2): 259-268, (1999).
- [5] Markworth, A.J., Ramesh, K.S., Parks, Jr.W.P., "Review: modeling studies applied to functionally graded materials", Journal of Materials Science, 30(3): 2183-2193, (1995).

- [6] Nemat-Allal, M.M., Ata, M.H., Bayoumi, M.R., Khair-Eldeen, W., “Powder metallurgical fabrication and microstructural investigations of Aluminum/Steel functionally graded material”, *Materials Sciences and Applications*, 2(5): 1708-1718, (2011).
- [7] Timesli, A., “Analytical Modeling of Buckling Behavior of Porous FGM Cylindrical Shell Embedded within an Elastic Foundation”, *Gazi University Journal of Science*, 35(1): 148-165, (2022).
- [8] Boğa, C., “Effect of Inhomogeneity Constant on Equivalent Stresses in Elastic Analysis of Hollow Cylinder Made from Functionally Graded Material”, *Gazi University Journal of Science*, 33(1): 201-212, (2020).
- [9] Miyamoto, Y., Kaysser, W.A., Rabin, B.H., Kawasaki, A., Ford, R.G. “Functionally Graded Materials: Design, Processing and Applications”, Kluwer Academic Publishers: Dordrecht/London/Boston, (1999).
- [10] Mahamood, R.M., Akinlabi, E.T. “Functionally Graded Materials”, Springer, (2017).
- [11] Gasik, M.M., “Functionally graded materials: bulk processing techniques”, *International Journal of Materials and Product Technology*, 39(1-2): 20-29, (2010).
- [12] Wu, X.L., Jiang, P., Chen, L., Zhang, J.F., Yuan, F.P., Zhu, Y.T., “Synergetic strengthening by gradient structure”, *Materials Research Letters*, 2(1): 185–191, (2014).
- [13] Shrikantha Rao, S., Gangadharan, K. V., “Functionally graded composite materials: an overview”, *Procedia Materials Science*, 5(1): 1291-1299, (2014).
- [14] Tejaswini, N., Babu, R., Ram, S., “Functionally graded material: an overview”, *International Journal of Advance Engineering Science and Technololgy*, 4: 183–188, (2013).
- [15] El-Galy, I.M., Saleh, B.I., Ahmed, M.H., “Functionally graded materials classifications and development trends from industrial point of view”, *SN Applied Sciences*, 1: 1378-1389, (2019).
- [16] Nikbakht, S., Kamarian, S., Shakeri, M., “A review on optimization of composite structures Part II: Functionally graded materials”, *Composite Structures*, 214: 83-102, (2019).
- [17] Zhang, Y., Ming-jie Sun, Zhang, D., “Designing functionally graded materials with superior load-bearing properties”, *Acta Biomaterialia*, 8: 1101-1108, (2012).
- [18] Uslu Uysal, M., Kremzer, M., “Buckling Behaviour of Short Cylindrical Functionally Gradient Polymeric Materials”, *Acta Physica Polonica*, A127: 1355-1357, (2015).
- [19] Uslu Uysal, M., “Buckling behaviours of functionally graded polymeric thin-walled hemispherical shells”, *Steel and Composite Structures: An International Journal*, 21(1): 849-862, (2016).
- [20] Uslu Uysal, M., Güven, U., “Buckling of Functional Graded Polymeric Sandwich Panel under Different Load Cases”, *Composite Structures*, 121: 182-196, (2015).
- [21] Uslu Uysal, M., Güven, U., “A Bonded Plate Having Orthotropic Inclusion in Adhesive Layer under In-Plane Shear Loading”, *The Journal of Adhesion*, 92: 214-235, (2016).
- [22] Dolgov, N. A., “Effect of the elastic modulus of a coating on the serviceability of the substrate-coating system”, *Strength of Materials*, 37(2): 422-431, (2002).

- [23] Dolgov, N. A., “Determination of Stresses in a Two-Layer Coating”, *Strength of Materials*, 37(2): 422-431, (2005).
- [24] Dolgov, N. A., “Analytical Methods to Determine the Stress State in the Substrate–Coating System Under Mechanical Loads”, *Strength of Materials*, 48(1): 658-667, (2016).
- [25] Rizov, V.I., “Non-linear fracture in bi-directional graded shafts in torsion”, *Multidiscipline Modeling in Materials and Structures*, 15(1): 156-169, (2018).
- [26] Rizov, V.I., “Analysis of Two Lengthwise Cracks in a Viscoelastic Inhomogeneous Beam Structure”, *Engineering Transactions*, 68(4): 397–415, (2020).
- [27] Broek, D., “Elementary engineering fracture mechanics”, Springer, (1986).